Trends in Mechanical Engineering& Technology
Volume 1, Issue 1, February, 2011, Pages 1-21.

SIMULATION OF COLD DIE COMPACTION ALUMINA POWDER

K. Mohammed Jasim Kadhim[1], Adil A. Alwan[2], Iman J. Abed[3]*

[1]Department of Production Engineering and Metallurgy, University of Technology, Baghdad, Iraq
[2]College of Engineering, University of Bayblon, Baibal, Iraq
[3]College of Engineering, University of Kufa, Najaf, Iraq

ABSTRACT

Compaction process was analyzed mathematically by predicting a steady-state mathematical model in order to give more description and understanding for the mechanism of this process. Numerical investigation has been carried out on axisymmetric cylindrical parts using the finite difference method with relaxation technique to examine the physical significance of constitutive model to produce the pressure gradients during compaction. The pressure distribution model is then typically coupled with empirical functions relating pressure and density to obtain a green density distribution at all nodes in the green compacts. The model has addressed the influence of frictional forces acting at the powder and die walls interfaces which dissipate the applied pressure throughout the compact. The effect of the compact geometry has a similar effect on the uniformity of green pressure and density distributions through the compact. It was found that a small aspect ratio resulted in a more uniform distribution than a higher aspect ratio. Therefore, the model seems to work better for the lower aspect ratio. The constitutive model predicts accurately the pressure and density distributions during compaction process.

Keywords: Finite difference method; Die compaction; Green density distribution; Aspect ratio; Alumina powder; Relaxation technique

***Author for Correspondence** email: alimohammed1957@yahoo.com

1. Introduction

Powder compaction is a commonly used technique in numerous fields, including the powder technology, geologic, pharmaceutical, and thermal battery industries (Portal, Euvrarde, Tailhades and Rousset, 1993). Uniaxial pressing consists of compacting the pressing powder contained in a rigid cavity, by applying a pressure in a single axial direction with one or more rigid punches. The various pressing techniques differ in the movement of the basic mould elements: top punch, bottom punch and die. In a single action, a uniaxial pressing pressure is applied through the top punch, which enters the cavity holding the pressing powder. After the compacting, the green piece and the top punch withdraw and the movement of the lower punch ejects the piece from the mould (Wagle, Engel, Liu and German, 2000). The compaction mechanism of different material powders is different from each other and the formation

of coherent compact is governed by a number of mechanisms (Mani, Tabil and Sokhansanj, 2004). The compaction of a given powder is conventionally divided into many stages and each stage is considered to be interrelated in terms of the physical and mechanical properties of powder particles.

The early stages of compaction are characterized by particle rearrangement (Morales, Aune, Seetharaman and Grinder, 2003; Lui, 2000) During this stage, particles rearrange themselves to form packed mass. The original particles retain most of their properties, although energy is dissipated due to interparticle and particle-to-die walls friction. The shape and initial porosity of powder particles are important material characteristics at the first stage, where sliding and plastic deformation or fractures play an important role. Generally, at the initial stage of compaction, the powder is moved inside the die reducing the porosity (Park, Han, Oh and Song, 1999). At high pressures, the particles are forced against each other even more and undergo elastic and plastic deformation, thereby increasing interparticle contact. Further densification during compaction takes place due to the mechanical interactions at the contact between neighboring particles. The final stage is considered to be almost entirely due to cold working of the bulk material and is affected by deformation and work hardening of particles Aydin, Briscoe and Sanliturk, 1996; Bejarano, Rieva and Prado, 2003; Chtourou, Guillot and Gakwaya, 2002; Chtourou, Guillot and Gakwaya, 2002; Lee and Kim, 2002; Lewis and Khoei, 1998; Michrafy, Ringebacher and Tchoreloff, 2002; Pivinskii, Dyakin and Dyakin, 2006; Shinohara, Okumiya, Hotta, Nakahira, Naito and Uematsu, 1999; Grigor'ev, Maiboroda, Panfilov and Shtern, 2003; Portal, Euvrard, Tailhades and Rousset, 1999; Mujahid, Gureshi and Islam and Khan, 1998). Many studies have been made to determine the mechanisms involved during compaction process. The finite element method has been widely used to simulate powder compaction (Secondi, 2002) and Gaboriault, 2003). Therefore, the present research is an attempt to understand the compaction phenomenon through developing a mathematical model. An axisymmetric finite difference steady state mathematical model has been developed to simulate the complete pressure response of the system.

2.Constitutive models for powder technology

Various approaches to model the compaction processes using finite element methods were available in literature. Many kinds of powder compaction equations have been proposed. Biba, Keife and Stahlberg (1993) studied theoretically for plane-strain conditions for uniaxial compaction of powders. The analysis is being focused upon the material flow into the holes between the powder particles. The original powder material is assumed to be building up of close packed cylinders of equal size. The investigation is carried by means of step-wise calculation. It is based upon a finite element approach. The agreement between the material flows as determined from plasticine experiments and that from the finite element analysis, which latter incorporates the plasticine constitutive equation is good. Theory and experiment are in acceptable agreement also in respect of the step-wise change of shape of the boundary surface defining the holes. It has been found that, the material flows are very sensitive to the mechanical properties of the

material, such as the flow stress and its dependence of the strain rate.

It has been shown that, during pulse loading, high densities close to corresponding to the nonporous state can be attained due to inertia effects (Boltachev, Volkov, Ivanov and Paranin; 2008). The influence of the initial radial dimensions of the rod-powder-medium system on the compaction process was analyzed. The problem was found to be scale invariant under various constrains imposed on the ratio of the characteristic dimensions. In addition, cold die compaction has been theoretically modeled of powder materials based on the axisymmetric solution of the large deformation (Al-Qureshi, Galiotto and Klein; 2005). The model produces an expression relating the green density of the collect to the applied pressure. The analysis takes into account the internal (restricted movements) coefficient of friction between the particles and the container-compacted powder interface friction. The yield stress of the materials plays a major and fundamental role in the final strength and density of the final compact part. Internal imperfections, especially internal cracks are probably the greatest and most expensive quality problems experienced by the powder metallurgy industry (Krezalek and Sivakumar; 1995). Majority of these imperfections arise, due to poor or insufficient powder flow in some regions of the compact and is introduced to the product during compacting of powder to green stage. Analysis of possibilities of introduction of imperfections requires the powder movement to be quantified. The application of finite element method may take design of powder metallurgy parts of complex geometries easier by evaluating different designing options and possibility of internal cracks introduced during compaction operation which can be analyzed and eliminated.

An expression related the green density and porosity of the compact during cold die compaction of powder as a function of process parameters have been analyzed (Al-Qureshi, Soares, Hotza, Alves and Klein; 2008). The analysis takes into account the internal coefficient of friction between the particles and the powder/container interface friction and the work hardening effect of the particles. Compression between experimental and theoretical distributions demonstrated remarkable agreement for all the tested conditions for different work hardening behavior of the particles. The finite element method has been used to study the effect of sand shell size on compaction and shape change during compaction of billets formed from the hot products of self-propagation high-temperature synthesis (Amosov, Rodchenko, Fedotov and Ermolenko; 2004). The extreme nature has also been established for the change in billet density in relation to shell thickness which governs its reserve of compressibility.

Appropriate structural model of powder compaction may suggest that the contact nature of plastic deformation of a powder body takes account. It has been shown that in averaging local stresses and strain rates, the volume of averaging can be presented as combination of straight cylinders constructed at all contact areas of a particle and having a common nucleus formed by the intersection of cylindrical bodies (Fedotov and Krasnoshchekov; 2005). The contact-rod model satisfies boundary conditions for the poured state of powder and it is good agreement with experimental data for isostatistically compacted metal powders. The shock compacted powders modeling of

the compaction mechanism has studied by Mamalis, Vottea and Manolakos (2001). It has been calculated this has shown that there is a great interest for explaining and understanding the densification mechanisms. Static and dynamic compaction techniques are useful for fabrication of components of various geometries, the description of the mechanisms of the process is very important. Thus, the finite element method is found as a powerful tool for predicting the compaction process and the deformation behavior of porous materials. A new mechanical model has been developed by Zhou, Chen, Zhao, Shao and Xia; 2002) for powder metallurgy compaction.Various amount of voids can be introduced into a continuous solid, therefore, the porosity can be conventionally controlled. The elastic-plastic finite element method was used to analyze the sintered powder material. A developed model has been applied to simulate compressing of a sintered cylinder. The plastic deformation of a metallic material is mostly caused by the slipping of the crystal lattice.

An algorithm for simulating the isostatic compaction of powders with dispersed spherical particles has also been studied (He and Ekere; 1998). The simulation results show that both the packing density and the average contact number are highly dependent on the particle dispersion. A double-surface plasticity model, based on a combination of a convex yield surface consisting of a failure envelope, such as a Mohr-Coulomb yield surface and, a hardening cap mode has been developed (Lewis and Khoei; 2001) for the nonlinear behavior of powder materials in the compact of a generalized plasticity formulation for the description of cyclic loading. A new expression for calculating the effective pressure acting on contacts between particles in powder aggregates underuniaxial compression has been proposed by Montes, Cintas, Rodriguez and Herrera (2003). The developed equation is a function of both the degree of porosity and the minimum packing porosity. The latter is roughly identical with the tap porosity and describes with some accuracy the pore structure in the powder or compact. It has also recognized that kinetics were important for compaction during hot pressing in a rigid die, and the change in density distribution (Grigor'ev, Maiboroda, Panfilov and Shtern; 2003). Irreversible solid phase strain accumulations, and equivalent stresses were very important to be studied by means of the finite element method. The die compaction of powders evaluated using spatially fixed finite element has been proved that the material constitutive behavior can be described by the theory of elastoplasticity (Brekelmans; 1990).

The basic equations of plasticity have been established to be very effective to derive a general algorithm for the implementation of a set of well-known constitutive models for porous materials (Justino, Alves, Llein and Al-Qureshi; 2006). The set of models were modified successfully to incorporate not only an isotropic work hardening, but also the coupling of the constitutive equations with the porosity at the material. It has been found that, the comparative analysis, performed with the given set of porous material models, shows a large difference in the response of the different models. A new experimental and theoretical investigation of the granular-medium shock-wave compaction process has been investigated by Boltachev, Volkov, Ivanove and Kargordov (2009). The mathematical model described the energy dissipation, which is stipulated by the work made to compact the powder, considering the loss for the non-ideal reflection of the shock wave from the

discontinuity surface on the borders of the body being compacted. A one-parameter equation that describes pressing of ceramic powders in the dimensionless coordinates relative pressing pressure-relative density of the compact was suggested by Khasanov, Dvilis and Sokolov (2001). It was shown that the boundary conditions are correctly obeyed for such an equation. The correctness of the initial conditions is provided by the developed method for plotting compaction curves. The finite element based plasticity model on porous material for metal powder forming processes may also be implemented (Biswas; 2005). It has been used to analyze stress state and kinematical constraint imposed on the test specimens with simple geometries. The overall picture of the powder pressing process seems to be very captured with the present computational model over a wide range of applied load.

It has been shown that from above investigations that several relationships between compaction pressure and green density have been proposed. The high number of relationships presented in literature reflects the complexity of the process. It is believed that the compaction process is difficult to generalize because it depends on a large number of parameters which are hardly to be completely adjustable. Some models took into account the powder characteristics, which include particle size, shape, and surface finish, while others incorporate material properties such as hardness or plasticity Secondi; (2002).

A fundamental understanding of the physical mechanisms that govern the powder compaction is central to the economics of powder technology. Hence, compactions modeling have received significant attentions over the last years (Gaboriault; 2003). There are two main approaches for compaction modeling namely micro-mechanical or discrete element method (DEM) and macro-mechanical method which considers the discrete nature of the powder particles. These “particulate” models describe how the basic physical laws affect the movement of individual powder particles. Micro-mechanical modeling describes the particle-particle and particle-wall interactions that take place when powder is compacted. Information pertinent to such modeling may include the average number of contacts, volume fraction of particles, contact area and center-to-center distances of adjacent particles. On the other hand, the macro-mechanical model treats the powder volume as a continuum. These continuum models describe how the pressure and density distributions within the compacting powder bed depend on the relevant powder properties and geometry during the compaction.

The macro-mechanical approach is the predominant modeling technique applies for powder compaction. The macro-mechanical model provides useful engineering information such as density distribution and post-compaction shape. Mathematically, macro-mechanical model involves the solution of a boundary value problem with partial differential equations for equilibrium (Gaboriault; 2003 and Mahoney and Readey; 1995). The micro-mechanical model provides information about the local behavior of the powder. The steady state pressure distribution is governed by the Laplace’s equation:-

$$h^2 \alpha \frac{\partial^2 P}{\partial r^2} + \frac{h^2 \alpha}{r} \frac{\partial P}{\partial r} - \frac{\partial^2 P}{\partial z^2} = 0 \qquad (1)$$

Trends in Mechanical Engineering& Technology
Volume 1, Issue 1, February, 2011, Pages 1-21.

The term steady state problems pertain to problems that describe steady state of systems that do not vary with time. The die wall was modeled as a rigid surface made of elastic material. During compaction at room temperature, the punches move at a slow rate, dynamic effects were neglected and no thermal effect was considered.

Two dimensional steady state model is in the radial and depth direction. For this model, P = (r, z) as represented in equation (1). This equation was solved using the following initial and boundary conditions:
Initial condition
P(r, z, 0) = 0 at time = 0 (2)
Boundary condition when time > 0
P(0, 0) = Pa (3)
The pressure at point P (0, 0) is equal to applied pressure (Pa)
P(r, 0) = applied pressure, at top of the compact (4)

$$p(0,z)=p_a*\exp(-4*\alpha*\mu*z(j)/D) \quad (5)$$

At the central axis, the axial compacting pressure at any depth in the compact is given by:

$$p(R,z)=p_{(1,j)}*\exp(-4*\alpha*\mu*z(j)/D)+\alpha*\mu*p_a \quad (6)$$

At the die Wall, during single action pressing (only from the top), the upper part of the green compact slides on the die. It is submitted to a normal load from the punch and simultaneously to a shear stress due to friction at the die wall effect Ready, Mahoney and Ewsuk; 1995 and Crawford and Sprevak; 1984).

$$p(r,L)=\%p_a*\exp(-4*\alpha*\mu/D)*r(i) \quad (7)$$

The pressure is dissipated from the top of the compact to the bottom. It depends on aspect ratio and coefficient of friction, the value is variable between 20 - 90%, this is reported by references (Pease III; 2005, Collins II; 2003 and Brewin, Coube, Doremus and Tweed; 2008). Boundary conditions are represented in Fig.1.

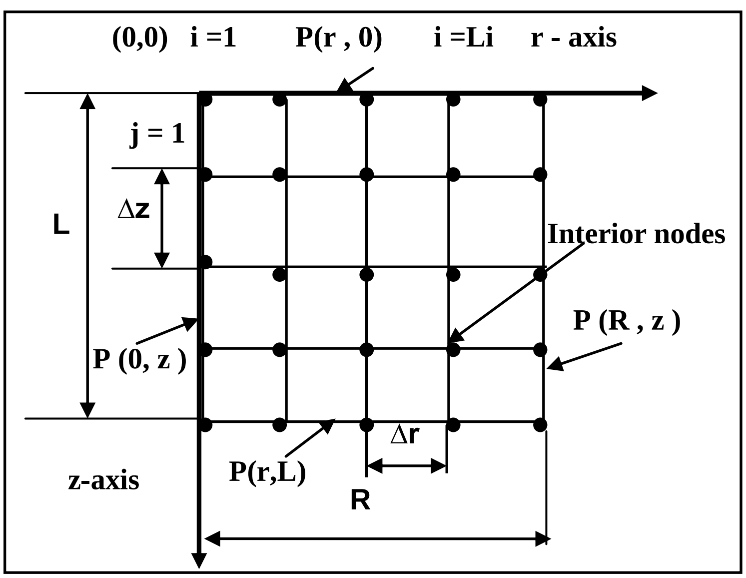


Fig. 1: Boundary conditions of material

Trends in Mechanical Engineering& Technology
Volume 1, Issue 1, February, 2011, Pages 1-21.

It is necessary to use the finite difference approximation to the partial differential equation system (PDEs), so that the problem could be solved by a computer. It has been considered an approximation in the region over which have laid an orthogonal grid with an equal spacing (the distance between neighboring points). The indices i and j will be used for indicating the points along the r and z directions. The distances between the points in the established grid are Δr, Δz. The grid is represented in Fig. 2.

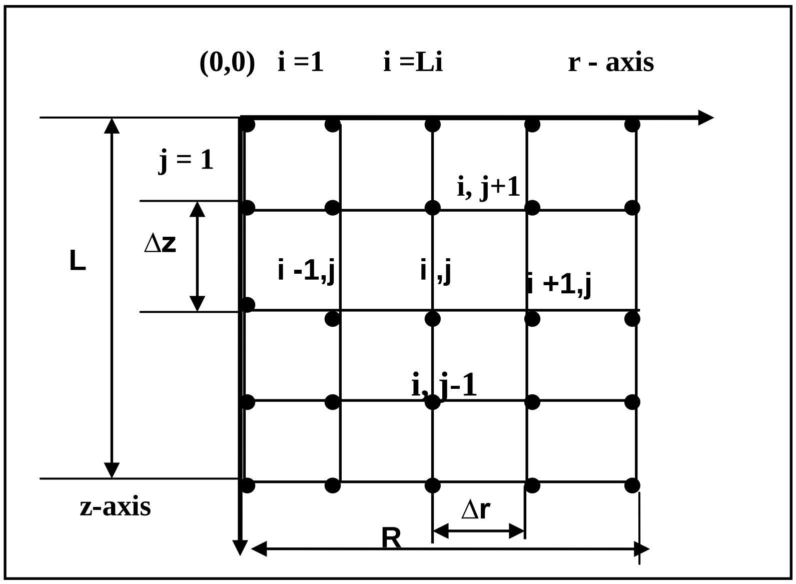


Fig. 2: Computational grid of the cylindrical model.

The central-difference scheme will be used to approximate the second derivatives of pressure in space:

$$\frac{\partial^2 p}{\partial r^2} = \frac{p_{i+1,j} - 2p_{i,j} + p_{i-1,j}}{\Delta r^2} + 0\left(\Delta r^2\right) \quad (8)$$

$$\frac{\partial^2 p}{\partial z^2} = \frac{p_{i+1,j} - 2p_{i,j} + p_{i-1,j}}{\Delta z^2} + 0\left(\Delta z^2\right) \quad (9)$$

The first order of accuracy for space is approximated by backward difference scheme:

$$\frac{\partial p}{\partial r} = \frac{p_{i,j} - p_{i-1,j}}{\Delta r} + 0\left(\Delta r\right) \quad (10)$$

The finite difference form of the governing equation (1) is:

$$h^2 \alpha \frac{p_{i+1,j} - 2p_{i,j} + p_{1-i,j}}{\Delta r^2} + \frac{h^2 \alpha}{r(i)} \frac{p_{i,j} - p_{i-1,j}}{\Delta r} - \frac{p_{i,j+1} - 2pi,j + p_{i,j-1}}{\Delta z^2} = 0 \quad (11)$$

Assuming that $\Delta r = \Delta z$, then equation (11) becomes:

$$h^2\alpha\left(p_{i+1,j}-2p_{i,j}+p_{i-1,j}\right)+\frac{h^2\alpha\Delta r}{r(i)}\left(p_{i,j}-p_{i-1,j}\right)-p_{i,j+1}+2p_{i,j}-p_{i,j-1}=0 \quad (12)$$

$$h^2\alpha\left(p_{i+1,j}\right)+p_{i,j+1}-p_{i,j-1}-\left[h^2\alpha-\frac{h^2\alpha\Delta r}{r(i)}\right]p_{i-1,j}=\left[2h^2\alpha-2-\frac{h^2\alpha\Delta r}{r(i)}\right]p_{i,j}$$

(13)

$$p_{i,j}=\frac{h^2\alpha\left(p_{i+1,j}\right)+p_{i,j+1}-p_{i,j-1}-\left[h^2\alpha\frac{h^2\alpha\Delta r}{r(i)}\right]p_{i-1,j}}{\left[2h^2\alpha-2-\frac{h^2\alpha\Delta r}{r(i)}\right]}. \quad (14)$$

Finite difference method is devoted to basic techniques for solving elliptic PDEs. The principles of stability analysis with numerical schemes are discussed by Fu, Jiang, Lannutti, Wagoner and Daehn (2002).

3.Numerical solution of finite difference equations

Most numerical solutions of the Laplace equations systems have been studied. For example in the present work equation (1) has 20-by-5 grids which involve 100 linear algebraic equations. Solution techniques to these types of equations were discussed by other investigators Shima and Saleh; 1993). Because they are prone to round off error, elimination methods are not usually employed for such systems. In addition, it is noticed that there is a maximum of five unknown terms per line in equation (1). For larger–sized grids, this means that a significant number of terms will be zero. When applied to such sparse systems, elimination methods waste great amounts of computer memory storing these zeros.

For the aforementioned reasons, Elliptic PDEs are usually solved with approximate method. The most commonly employed approach is Gauss–Seidel iteration (Shima and Saleh; 1993). The finite difference equation is applied at each node, node by node. With each calculation, the updated value from the previous node is used. The calculation may also incorporate the method of relaxation. The calculations are continued until repeated iterations fail to change the pressure distribution within a specified amount. This procedure will eventually converge on a stable solution. Over relaxation is often employed to accelerate the rate of convergence by applying the following formula for each iteration:

$$p_{i,j}{}^{new}=w.p_{i,j^{new}}+(1-w)p_{i,j^{old}} \quad (15)$$

Trends in Mechanical Engineering& Technology
Volume 1, Issue 1, February, 2011, Pages 1-21.

STM JOURNALS

where $p_{i,j}$ and $p_{i,j^{old}}$ are the values of Pi,j from the present and the previous iterations respectively and *w* is a weighting factor

which is set between 1 and 2. As with the conventional Gauss-Seidel method, the iterations are repeated until the absolute values of all the percent relative errors, εai,j, fall below a prespecified stopping criterion, ε_s. These percent relative errors are estimated by:

$$|(\varepsilon_a)| = \left| \frac{p_{i,j^{new}} - p_{i,j^{old}}}{p_{i,j^{new}}} \right| \times 100. \quad (16)$$

At in present work, the over relaxation is employed with a value of 2 for the weighting factor and iterate to $\varepsilon_s = 1$

4.Prediction density gradients

In spite of high degrees of surface finish on the tool set, friction exists between the powder and the tool components. Axial forces applied by the compaction load cause radial forces to be generated at the die walls. A differential pressure distribution during compaction produces a density gradient in the green parts. To predict the relative green density of the compact, the following equation was used:-

$$\rho = \rho_\circ + k.p^{1/3} \quad (17)$$

where ρ is a relative density, ρ_o is an initial relative density, P is an applied pressure and k is a constant reflect variations in material properties such as hardness and plasticity. *k* appears to be a material constant. Soft and ductile powders have higher *k* values than hard and brittle powders. This descriptive property of the constant *k* for deformation behavior of the material leads to the following correlation between *k* and the yield strength (σ_y) Bejarano, Riera and Pracb; 2003):

$$\sigma_y = 1/3k \quad (18)$$

The reciprocal of the slope k has been found to reflect the yield pressure P_y of a material. This means that the yield pressure P_y of a material is equal to $3\sigma_y$ J. Scott and Kenkre; 1998 and Mahoney and Readey; 1995). For a compaction of alumina, this occurs between approximately 0.1 and 10 MPa (Shackelford and Alexander; 2001). At this stress, the granules comprising the powder begin to permanently deform by plastic strain and/or fracture. This corresponds to the beginning of stage III compaction. In modeling of prediction density is the value of σ_y = 5 MPa depending on data for Sandia National Laboratories Collins II; 2003).

5.Results and discussion

Numerous analysis and models have been found in the literature for investigating and predicting the compaction behavior of ceramic powders. It is important to note that such diagrams pertain only to the average properties of powder compacts. To better understand the significant issue of density variations within pressed powder compacts, models of pressure distribution which are obtained from an applied compacting pressure have been developed and implemented into a finite difference method.

The processing of an axisymmetric component has been simulated. Coupling pressure distribution functions with pressure-density relationship allows the development of model to predict density distribution. The intermediate stage model and the data for alumina of 94% purity are taken from industry teams with Sandia National Laboratories to develop a predictive model for a powder pressing and die design Ready, Mahoney and Ewsuk; 1995 and Mahoney and Readey; 1995).

Cylindrical dies were used in modeling due to their simplicity in operation. Four different aspect ratios (compact thickness-to-die diameter) were chosen: 0.38, 0.75,1 and 2 which reflected a wide range of typical operating conditions for spray dried alumina powder containing several percent of a methylcellulose binder. This gives approximately the initial compaction relative density 28% percent from the theoretical density. This allows comparing the results with the available experimental results for same powder. It is initial density is 1.036 g/cm^3; its maximum theoretical density is 3.97 g/cm^3 Shackelford and Alexander; 2001).

5.1. Effect of coefficient of friction

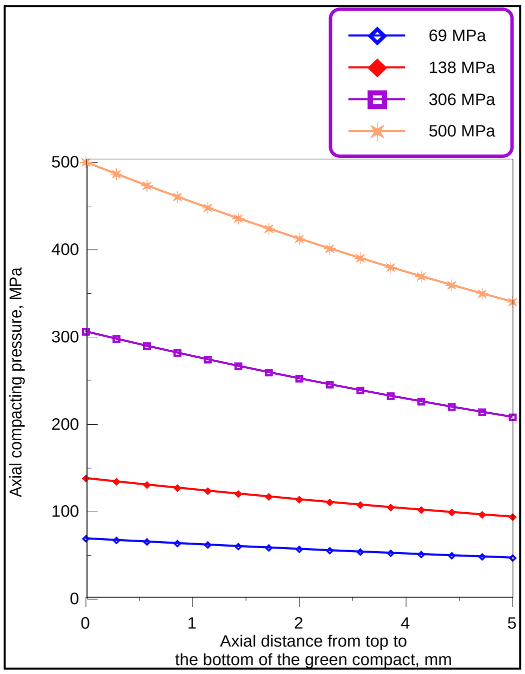


Fig. 3: The variations in axial compacting pressure with axial distance in alumina green compacts at aspect ratio, h = 0.38, $\alpha = 0.5$ and $\mu = 0.1$ with different pressing pressures

Figure 3 postulates the variations in pressure distribution predicted through the compact, along the top surface of the pressure distribution as a function of a radius; it exhibits a minimum at the centerline and increase toward the edge of the compact. Note that the corners near the moving portion of the die, where the pressure builds up are the highest. The pressure at the edges decreases with depth from the surface to the bottom of compact.

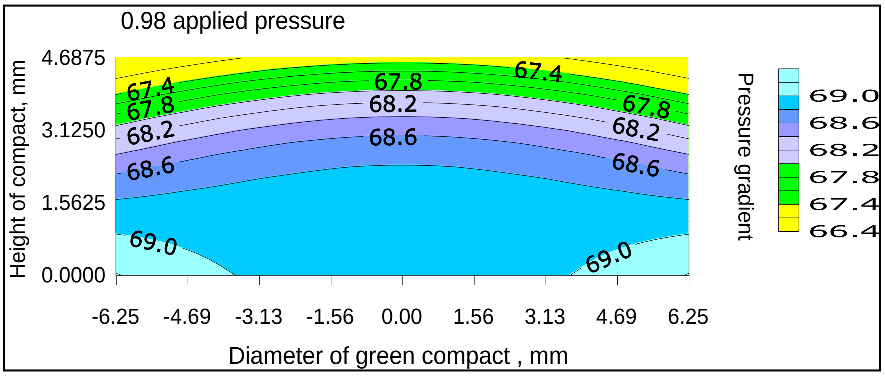


Fig. 4 Pressure contour maps for alumina green compact under compacting pressure 69 MPa, aspect ratio, h = 0.38, α = 0.1 and μ = 0.1.

Figure 4 shows the variation in pressure distribution predicted through the compact, along the top surface of the pressure distribution as a function of radius; it exhibits a minimum at the centerline and increase toward the edge of the compact. The corners near the moving portion of the die, where the pressure builds up are the highest and the region farthest from the moving part of the die, where the pressure is the lowest. When the coefficient of friction is increasing to 0.4 (Fig. 5), the pressure at the bottom of the compact reaches approximately 94% of applied pressure.

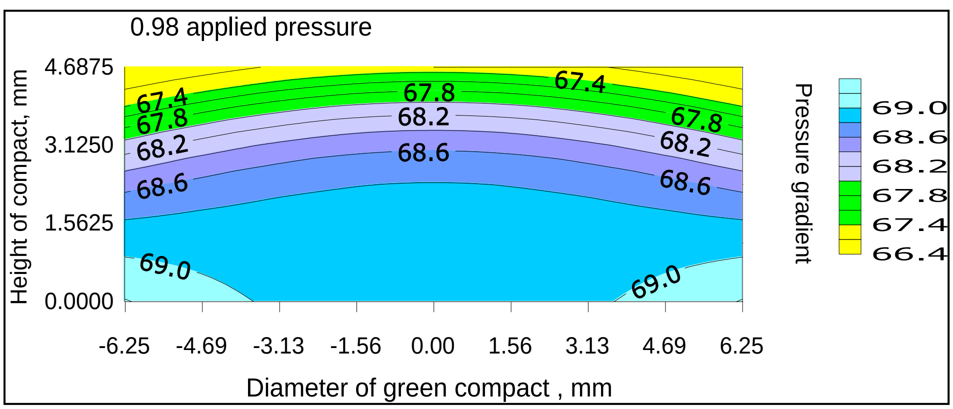


Fig. 5: Pressure contour maps for alumina green compact under compacting pressure 69 MPa, aspect ratio, h = 0.38, α = 0.1 and μ = 0.4.

Figure 6 shows the effect the coefficient of friction on the density distribution predicted from the compact parts. The variation in density (difference between the maximum and minimum densities) in the part increases with an increasing in friction value. The maximum relative density was predicted to be approximately 54.85% at the edge formed due to die wall friction of 0.1 at 69 MPa compacting pressure.

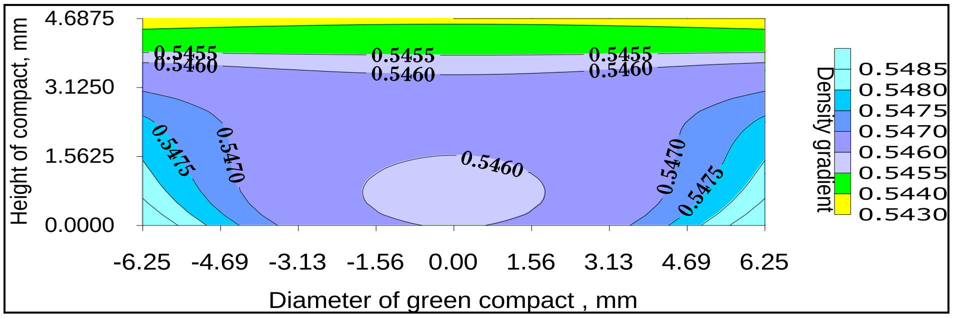


Fig. 6: Density contour maps for alumina green compact under compacting pressure 69 MPa, aspect ratio, h = 0.38, α = 0.1 and μ = 0.1.

5.2. Effect of aspect ratio

If pressure decreases exponentially through the compact, then the aspect ratio of the compact must also have a significant influence. To show this effect, it is assumed that the coefficient of friction, μ and radial to axial pressure ratio, α are constants during the simulation of the compaction process and consider only the effect aspect ratio.

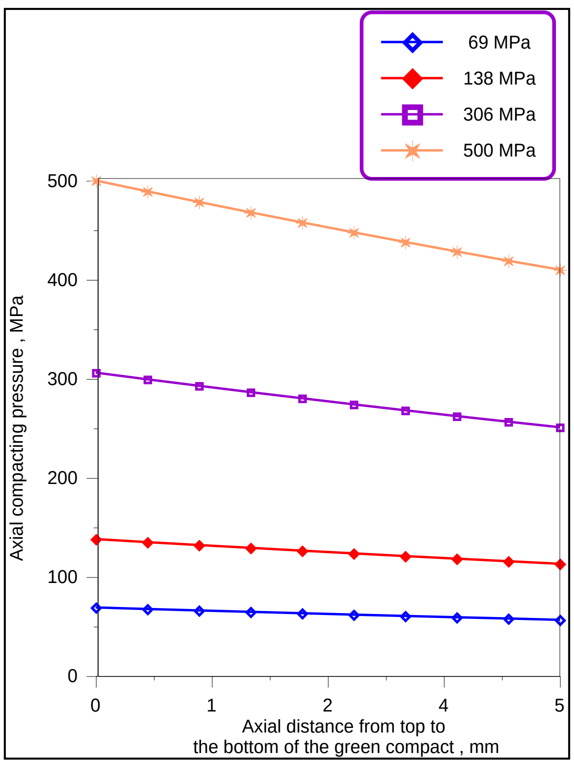


Fig. 7: The variations in axial compacting pressure with axial distance in alumina green compacts at aspect ratio, h = 0.38, α = 0.25 and μ = 05 at different pressing pressure.

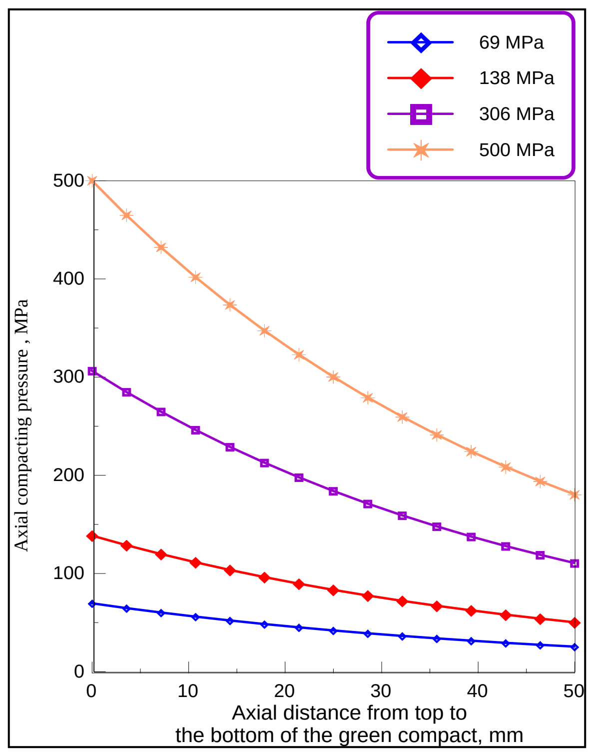


Fig. 8: The variations in axial compacting pressure with axial distance in alumina green compacts at aspect ratio, h = 2, α = 0.25 and μ = 05 at different pressing pressures.

Trends in Mechanical Engineering& Technology
Volume 1, Issue 1, February, 2011, Pages 1-21.

Figures 7 and 8 show the effect of compact geometry on axial compacting pressure with axial distance in alumina green compact as a function of aspect ratio with a radial to axial pressure ratio equal to 0.25, the coefficient of friction at die walls is equal to 0.5 at different compacting pressure 69, 138, 306 and 500 MPa. At an aspect ratio equal to 0.38, the pressure at the bottom of the compact is nearly 82% of the applied compacting pressure which transmitted to the bottom of the compact as shown in figure7. For aspect ratio h = 2, only 36% of applied pressure is transmitted to the bottom of the compact as shown in figure 8.

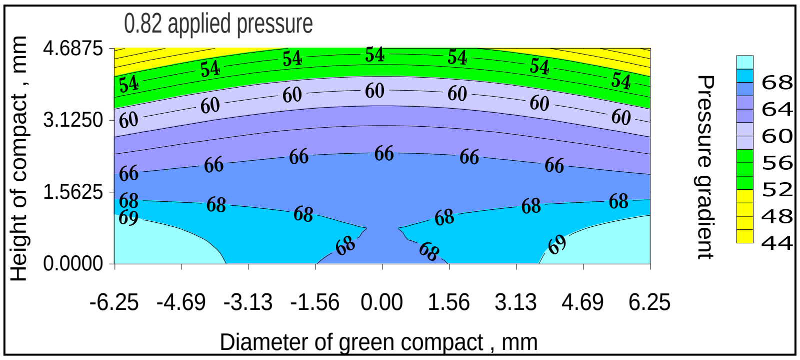


Fig. 9: Pressure contour maps for alumina green compact under compacting pressure 69 MP, aspect ratio, h = 0.38, α = 0.25 and μ = 0.5.

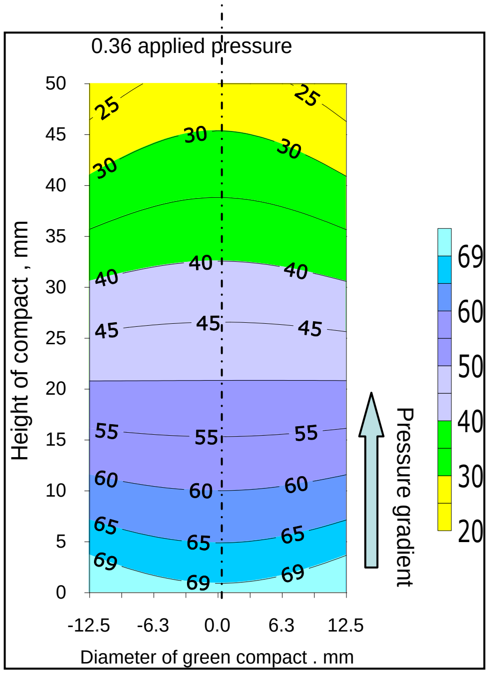


Fig. 10 Pressure contour maps for alumina green compact under compacting pressure 69 MPa, aspect ratio h = 2, α = 0.25 and μ = 0.5.

Figures 9 and 10 show the pressure distribution in the powder compact in different aspect ratios. It may be compared between them in order to explain the effect of aspect ratio on pressure distribution. Note, along the top surface, the pressure is a function of the radius. It is increasing from a minimum at the center to a maximum at the edge of the compact. Moreover, pressure decreases along the die wall from a maximum at top edge to a minimum at bottom of compact. At the low aspect ratio (Fig. 9), the variation in pressure distribution is low (about 36%). While at the high aspect ratio, the variation in pressure distribution reaches to 70%. Also, it has been observed from these figures that no contours closed occur. Decreasing the aspect ratio resulted in increased in the rate of diffusion of the wall boundary conditions into the compact.

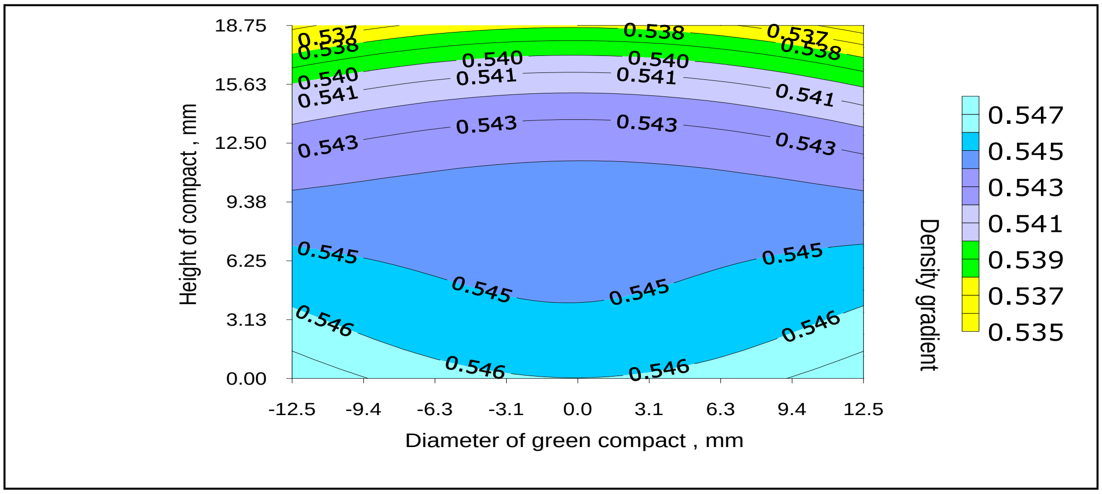


Fig. 11: Density contour maps for alumina green compact under compacting pressure 69 MPa, aspect ratio, h = 0.75, α = 0.1 and μ = 0.25.

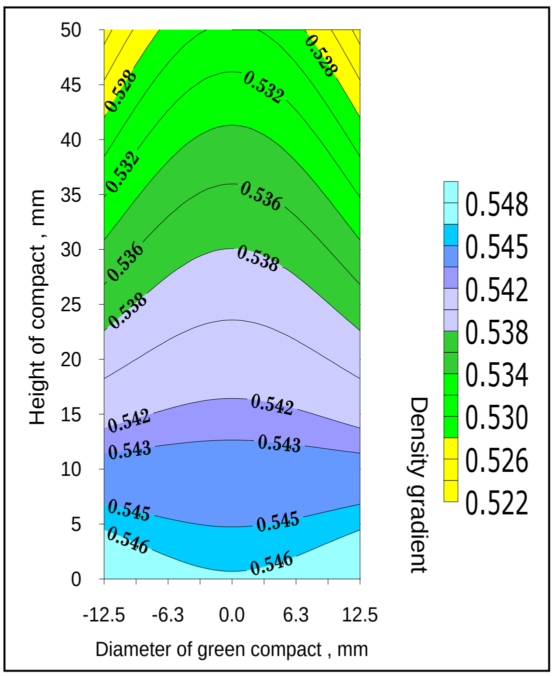


Fig. 12: Density contour maps for alumina green compact under compacting pressure 69 MPa, aspect ratio, h = 2, α = 0.1 and μ = 0.25.

Figures 11 and 12 demonstrate that the contour plot of the distribution obtained is described the results of the finite difference for density distributions. It shows that at an aspect ration of 0.75 and a low pressure (Fig. 11), there are well defined regions of high density. At the top of compact, this increases with the radius to a maximum value. Fig.12 shows the prediction density at the die wall regions. Maximum relative density of 54.7% is at the die wall and the minimum relative density of 53.5% is at the bottom of the compact at a compacting pressure of 69 MPa. At the high aspect ratio equal to 2 (Fig. 12), the difference between minimum and maximum densities is approximately 52.2– 54.8% at a pressure of 69 MPa.

Trends in Mechanical Engineering& Technology
Volume 1, Issue 1, February, 2011, Pages 1-21.

5.3. Effect of radial to axial pressure ratio

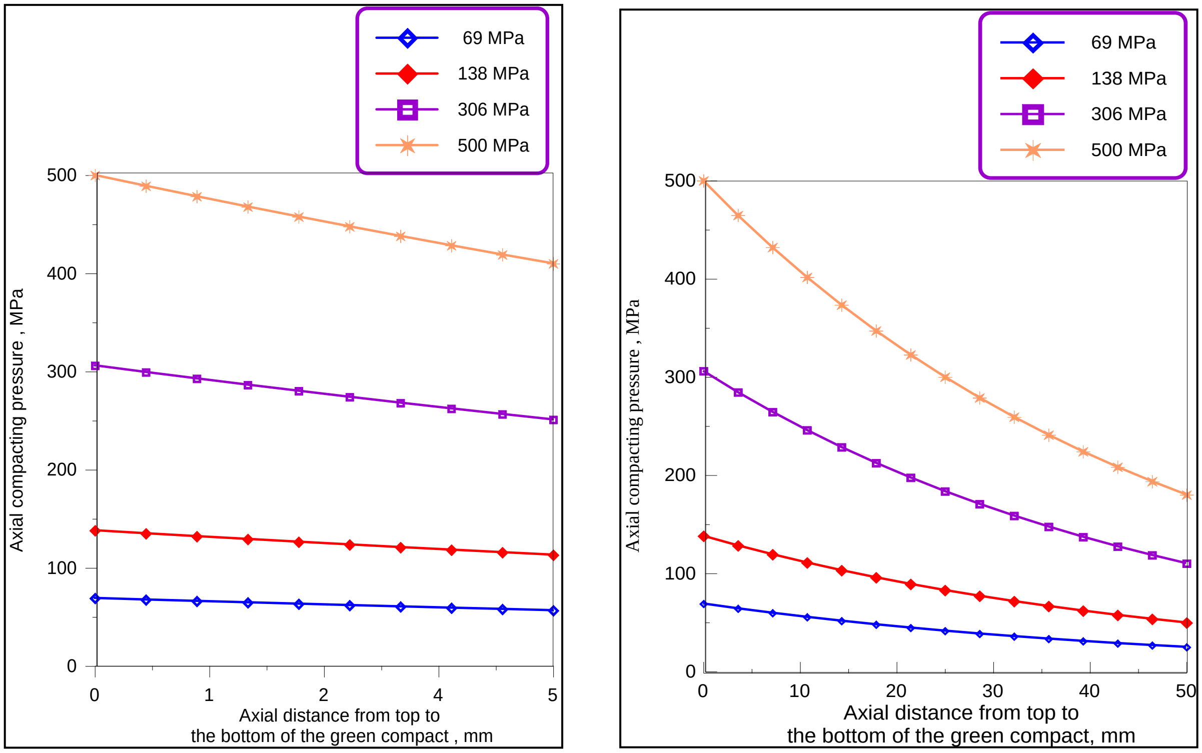


Fig. 13: The variations in axial compacting pressure with axial distance in alumina green at aspect ratio, h = 2 and μ = 0.4 at different radial to axial pressure ratio, α (a) 0.25 and (b) 0.5.

Figure13 describes the variation in axial compacting pressure with axial distance in alumina green compact as a function of radial to axial pressure ratios of 0.25 and 0.5 at aspect ratio of 2 and coefficient of friction, μ 0.4. It was observed from Fig. 13 that the axial applied pressure decreases exponentially with the depth of compact. The radial to axial pressure ratio has qualitatively similar effect on the density differences as do the coefficient of friction. When the radial-to-axial pressure ratio is equal to 0.25 (Fig. 13a); the pressure at the bottom of compact is nearly 45% of the applied compacting pressure transmitted to the bottom of the compact. Increasing the radial-to-axial pressure ratio up to 0.5 (Fig. 13b); the pressure at bottom of compact was nearly 20% of the applied compacting pressure transmitted to the bottom of the compact. Therefore, increasing the radial-to-axial pressure ratio is leading to a higher decrease in axial applied pressure at bottom of green compact. Figure 14 shows the effect of radial-to-axial pressure ratio on pressure gradient, the difference in a maximum and a minimum pressure values between top and bottom of compact is approximately 10%. Increasing the radial-to-axial pressure ratio to 0.25 increases the pressure gradient up to 25%. At a higher radial-to-axial pressure ratio (Fig. 15), the pressure gradient is about 36%.

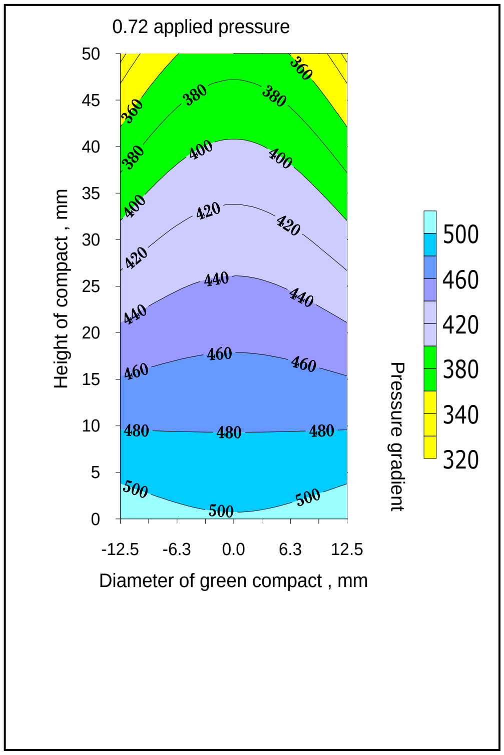


Fig.14: Pressure contour maps for alumina green compact under compacting Pressure 500 MPa, aspect ratio, h = 2, α = 0.1 and μ = 0.1.

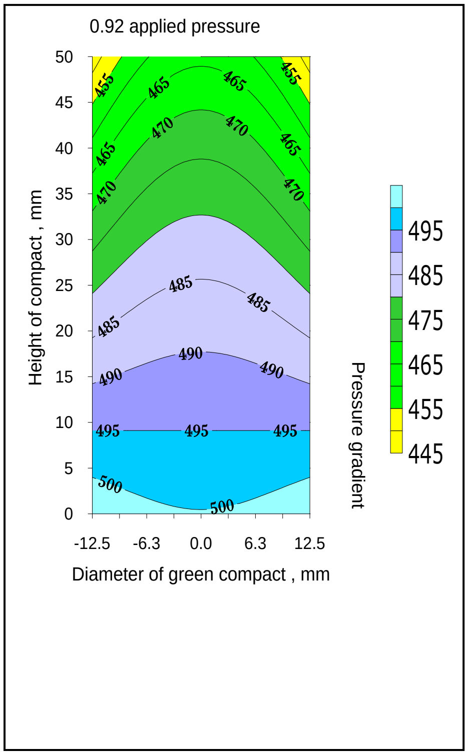


Fig. 15: Pressure contour maps for alumina green compact under compacting pressure 500 MPa, aspect ratio h = 2, α = 0.4 and μ = 0.1.

Figure 16 explains the effect of increasing the radial-to-axial pressure ratio on the resulting density variation for three values of radial-to-axial pressure ratios. It can be seen from this figure that several observations in prediction the variation of the density for 94% alumina under compacting pressure of 500 MPa are seen. Firstly, near the die-wall region, the density decreases in the axial direction from top to the bottom of the compact. The highest density is found at the top of the compact at the die wall. The lowest density is at the bottom of the compact at the die wall. Secondly, in the radial direction, the model predicted shows an increasing in the density from central axis to the edge of the compact in the top region of the sample.

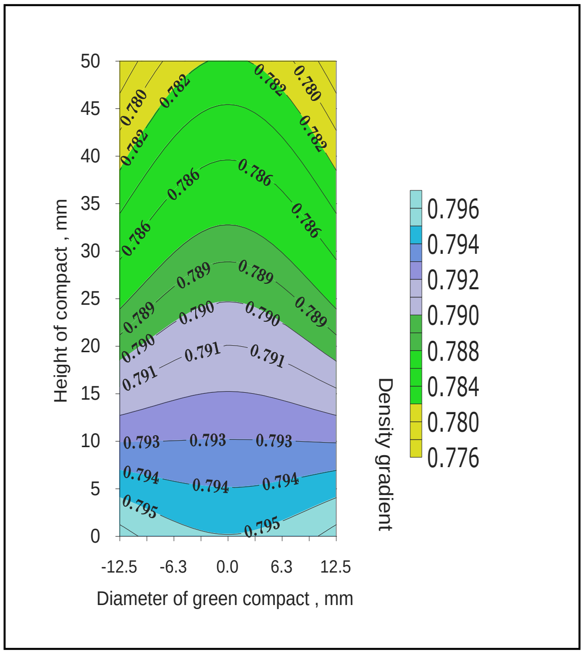


Fig. 16: Density contour maps for alumina green compact under compacting pressure 500 MPa, aspect ratio, h = 2, α = 0.1 and μ = 0.1.

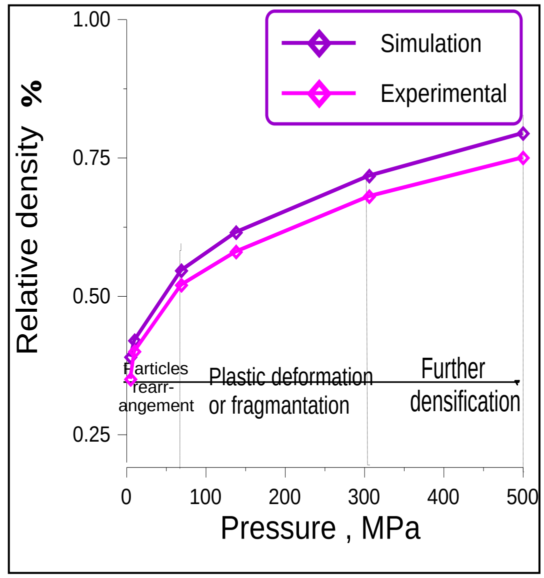


Fig. 17: Simulation and experimental Pressure–density diagrams for alumina green compact at different compacting pressure.

5.4. Prediction pressure - density of green compacts

Figure 17 shows the relationship between the compaction pressure with relative density for simulation and experimental results. It can be seen that the relative density increases with increasing compacting pressure; the pores decrease with increasing the compacting pressure. The pressure-density relationship shows that there is initially a large increase in density during the low pressure applied. This may be due to the initial rearrangement of particles. As the density of the part increases, the curve levels are indicating not much change in density when pressure is applied. It is appeared that the first region at low pressure is due to particles rearrangement. The second region appears to be a linear, where a brittle fragmentation occurs. The third region shows the change in density with increasing pressure.

6. Conclusions

1. The simulation of predicting pressure shows experimental data has an excellent agreement with computational results obtained using this models.
2. The compact geometry has effect on uniformity of green pressure–density distributions through the compact. Small aspect ratio has a more uniform than higher aspect ratio.
3. Small aspect ratio has a more uniform than higher aspect ratio due to low density variations in low aspect ratio. Therefore the model seems to work better for the lower aspect ratio.
4. Friction plays an important role in determining pressure distributions. The pressure at die wall decreases gradually from top to the bottom of the compact because of the pressure gradient.

5. The variations in axial compacting pressure with axial distance increasing with increasing the coefficient of friction. Increasing in radial pressures gives rise to increased friction forces at die wall, therefore the difference in maximum and minimum in pressure values between top and bottom of compact increase.

7.Acknowledgments

One of the authors (MJK) acknowledges Prof. A.R. Boccaccini, Imperial College of Science, London, Scholar Rescue Fund (SRF) USA and CARA, Uk for interest and helpful during his fellowship.

8.References

1. Al-Qureshi H. A. et al. *Journal of Materials Processing Technology* 2005. 166. 135-153p.
2. Arris J. E. et al. *Society for the Advancement of Materials and Process Engineering* (SAMPE) Covina, CA, USA. 622-634p.
3. Aydin I. et al. *Powder Technology* 1996. 89. 239-254p.
4. Al-Qureshi H. A. et al. *Journal of Materials Processing Technology* 2008. 199. 417-424p.
5. Amosov A. P. et al. *Powder Metallurgy and Metal Ceramics* 2004. 43. 229-235p.
6. Brewin P. R. et al. *Modeling of powder die compaction* Published by Springer, First Edition. 2008.
7. Bejarano A et al. *Journal of Materials Processing Technology* 2003. 143-144:34-50.
8. Biswas K. *Journal of Materials Processing Technology* 2005. 166. 107-115p.
9. Biba N. V. et al. *Journal of Materials Processing Technology* 1993. 36. 141-145p.
10. Boltachev G. S. et al. *Journal of Applied Mechanics and Technical Physics* 2008. 49. 336-339p.
11. Boltachev G. S. et al. *Acta Mechanica* 2009. 204. 37-50p.
12. Brekelmans WAM "*Journal of Materials Processing Technology* 1990. 24. 33-42p.
13. Chtourou H. et al. *International Journal of Solids and Structures* 2002. 39. 1059-1075p.
14. Chtourou H. et al. *International Journal of Solids and Structures* 2002. 39. 1077-1096p.
15. Crawford R. J. and Sprevak D. *European Polymer Journal* 1984. 5. 441-446p.
16. Fedotov A. F. and Krasnoshchekov P. I. *Powder Metallurgy and Metal Ceramics* 2005. 44. 420-425p.
17. Fu Y. et al. *Metallurgical and Materials Transactions* 2002. A33. 183-191p.

18. Collins II G. W. "Fundamental numerical methods and data analysis" *NASA Astrophysics Data System* (ADS) USA. 2003. 25-50p.

19. Grigor'ev O. N. et al. *Powder Metallurgy and Metal Ceramics* 2003. 42. 217-224p.

20. Gaboriault E. M. *The effects of fill-nonuniformities on the densified states of cylindrical green P/M compacts* MSc Thesis. Department of Mechanical Engineering, Worchester Polytechnic Institute, USA. 2003.

21. Grigor'ev O. N. et al. *Powder Metallurgy and Metal Ceramics* 2003. 42. 217-224p.

22. He D. and Ekere N. *Journal of Materials Science Letters* 1998. 17. 1723-1725p.

23. Justino J. G. et al. *Journal of Materials Processing Technology* 2006. 179. 44-49p.

24. Khasanov O. L. et al. *Refractories and Industrial Ceramics* 2001. 42. 37-40p.

25. Krezalek I. C and K. Sivakumar K. *Journal of Materials Processing Technology* 1995. 48. 421-427p.

26. Lui D. *Compaction studies of a particulate solid* MSc Thesis. The University of Queensland, Department of Chemical Engineering, Australia. 2000.

27. Lee S. C and Kim K. T. *International Journal of Mechanical Sciences* 2002. 044. 1295-1308p.

28. Lewis R. W. and Khoei A. R. *International Journal of Plasticity* 2001. 17. 1659-1692p.

29. Lewis R. W. and Khoei A. R. *Computer Methods in Applied Mechanics and Engineering* 1998. 159. 291-328p.

30. Mahoney F. M. and Readey M. J. *Applied mechanics modeling of granulated ceramic powder compaction. Conference:* 27 International Society for the Advancement of Materials and Process Engineering (SAMPE) Technical conference, Albuquerque, NM, USA. 10-12 Sep. 1995.

31. Mani S. et al. *Biosystems Engineering* 2004. 46. 355-361p.

32. Morales R. et al. *JOM: The Member Journal of TMS (The Minerals, Metals & Materials Society)* 2003. 55. 20-24p.

33. Michrafy A. et al. *Powder Technology* 2002. 127. 257-266p.

34. Mujahid M. et al. *Journal of* Materials *Engineering* and *Performance* 1998. 8. 496-500p.

35. Montes J. M. et al. *Journal of Materials Science Letters* 2003. 22. 1669-1671p.

36. Mahoney F. M. and Readey M. J. *Ceramic compaction models useful design tools or simple trend indicators* Conference: 97 Annual meeting of the American Ceramic Society, Cincinnati, OH, USA. 30 Apr - 1 May 1995.

37. Mamalis A. G. et al. *Journal of Materials Processing Technology* 2001. 108. 165-178p.

38. Pivinskii Y. E. et al. *Refractories and Industrial Ceramics* 2006. 47. 132-138p.

39. Park C. H. et al. *Powder Metallurgy* 1999. 42. 269–274p.

40. Portal G et al. *Powder Metallurgy* 1999. 1. 34-40p.

41. Pease III L. F. *Advanced Materials and Processes* 2005. 163:36-38.

42. Ready M. J. et al. "*Compaction of spray-dried ceramic powders: an experimental study of the factors that control green density"* International (SAMPE) Technical conference series. Edited R. J. Martinez, H. 1995. 27.

43. Secondi J. *Powder Metallurgy* 2002. 45. 213-217p.

44. Shinohara N. et al. *Journal of Materials Science* 1999. 34. 4271-4277p.

45. Shima S. and Saleh M. (1993) *Variation of density distribution in compacts in lose die compaction with powder characteristics, Advanced in powder metallurgy and Particulate materials, modeling design and computational methods* Nashville, Tennessee, USA. 16-19 May, 1993. 175-188p.

46. Scott J. V. and Kenkre V. *Physics Review E* 1998. 57. 5850-5857p.

47. Shackelford J. F. and Alexander W. *CRC Materials science and Engineering Handbook* Taylor and Francis Group. Third Edition. 2001. 103p.

48. Wagle G. S. et al. *International Conference on powder metallurgy and particulate materials (PM2TEC 2000)* New York city, NY, USA. May 30-June 3, 2000.

49. Zhou Z. Y. et al. *Journal of Materials Processing Technology* 2002. 129. 385-388p.

STM JOURNALS

Nomenclature

Symbol	Nomenclature	Units
P/T	Powder Technology	-
H	Height of compact	mm
R	Radius of compact	mm
D	Diameter of compact	mm
μ	Coefficient of friction	-
ρ_g	Green density	g/cm^3
ρ_t	True density	g/cm^3
W	Weight of the compact	g
L	Thickness of the compact	mm
ρ_r	Relative density	-
ρ_o	Initial relative density	-
P	Pressure	MPa
P_a	Applied pressure	MPa
ρ_1, ρ_2	Particle density of components of the mixture	g/cm^3
P_y	Yield Pressure	MPa
σ_y	Yield stress	MPa
h = H/R	Aspect ratio	-
T	Shear stress	MPa
A	Radial to axial pressure ratio	-
z-coordinate	Axial direction	-
r-coordinate	Radial direction	-
$P_{i,j}{}^{new}$	New value of pressure	MPa
$P_{i,j}{}^{old}$	Old value of pressure	MPa
W_i	Weighting factor	-
ε_S	Stopping Criterion	-
$W_{i,j}$	Relative error	-